JMEPEG (2005) 14:528-538
DOI: 10.1361/105994905X56106

1059-9495/$19.00

Effect of Boron and Carbon on the Fracture Toughness of IN 718 Superalloy at Room Temperature and 650 °C

Lin Xiao, Daolun Chen, and Mahesh C. Chaturvedi

(Submitted May 18, 2005; in revised form May 24, 2005)

The effect of B and C microadditions on the fracture toughness of IN 718 superalloy was investigated at room temperature (RT) and at 650 °C. At RT, the fracture toughness was observed to increase with increasing B and C concentrations. C had a relatively weak effect on the fracture toughness at 650 °C, but the influence of B was significant. At RT the highest fracture toughness value was obtained for the alloy with 29 ppm B and 225 ppm C at RT, and at 650 °C the alloy with 60 ppm B and 40 ppm C had the highest fracture toughness. An increase in the concentration of B to 100 ppm, however, resulted in a reduction in the fracture toughness at 650 °C. Fractographic observations showed that the formation and coalescence of microvoids was the predominant fracture mechanism at RT. In contrast, at 650 °C, the fracture surface exhibited intergranular cracking in the alloy with lower B concentrations and transgranular cracking coupled with fine dimples in the alloy with higher B concentrations. It is suggested that B impedes intergranular cracking by increasing the cohesion of grain boundaries and improving the grain boundary stabilization. The RT increase in the fracture toughness of the material caused by the addition of C is attributed to the formation of intergranular and intragranular carbides that increased the resistance to the plastic deformation.

Keywords fracture toughness, J integral, J_{IC}, K_{IC}, K_Q, microstructure

1. Introduction

IN 718 superalloy is being extensively used as a structural material in aerospace and space applications for manufacturing a variety of components such as gas turbine engine disks, blades and shafts, large structural castings, and powerhead components in the main engine of the space shuttle. Its advantages include excellent corrosion and oxidation resistance coupled with superior mechanical properties at elevated temperatures. In addition, IN-718 still possesses relatively good weldability and resistance to strain-age cracking because of the sluggish precipitation kinetics of its primary strengthening phase γ'' (Ref 1, 2). An understanding of the role of minor elements added to the base composition of IN 718 is essential for improving the mechanical properties of the alloy. In nickel-base superalloys, carbon additions are reported to form $M_{23}C_6$ and M_6C grain boundary carbide precipitates (Ref 1-6). When these intergranular carbides are present as discrete particles, they are reported to "pin" the grain boundaries and thereby inhibit grain boundary sliding at elevated temperatures. Conversely, when grain boundary carbides are present as a continuous film, they provide easy paths for crack propagation and thereby degrade high-temperature mechanical properties. Boron (B) is often added to IN 718 to improve the creep resistance (Ref 1, 2, 7, 8); however, it makes the alloy susceptible to heat affected zone (HAZ) liquation cracking or microfissuring by segregating at the grain boundaries during pre-weld heat treatment (Ref 9-12). Although a large number of investigations have been carried out to study the mechanical properties of IN 718 (Ref 13-18) and the effect of B on HAZ microfissuring (Ref 9-12), very limited work is available on the effect of B concentration on mechanical properties (Ref 19, 20), and the mechanism by which B improves the fracture properties of IN 718 is not fully understood. Hence, the objective of this study was to study the effect of B and C concentration on the fracture toughness of IN 718 at room temperature (RT) and 650 °C.

Lin Xiao and **Mahesh C. Chaturvedi,** Department of Mechanical and Manufacturing Engineering, University of Manitoba, Winnipeg, Manitoba R3T 2N2, Canada; and **Daolun Chen,** Department of Mechanical and Industrial Engineering, Ryerson University, 350 Victoria Street, Toronto, Ontario M5B 2K3, Canada. Contact e-mail: mchat@cc.umanitoba.ca.

2. Experimental Procedure

2.1 Materials and Heat Treatment

Four wrought 12.7 mm thick plate IN 718 based alloys, which had a similar base composition but contained different concentrations of B and C, were produced via a vacuum induction melting (VIM) + vacuum arc remelting (VAR) for this research by Special Metal Corporation (Huntington, WV) (12 and 29 ppm B) and by ALLVAC (Monroe, NC) (60 and 100 ppm B). The details of the melting and fabricating process have been reported elsewhere (Ref 19). The actual chemical composition of these alloys is given in Table 1.

Standard compact tension (CT) specimens with a width W of 50.8 mm and thickness B of 12.7 mm, were machined from the alloy plates in the T-L orientation (T - transverse direction or the direction of least deformation, and L - longitudinal direction or the direction of principal deformation) using electro-discharge machining (EDM) techniques. The specimens were heat treated with a commercial heat treatment (CHT). The CHT involved a solution anneal at 954 °C for 1 h and air cooling to RT. Then, the specimens were precipitation hardened by aging

Table 1 Composition of the selected IN 718 (wt.% unless designated ppm)

Alloy	Mn	Si	Cr	Ni	Co	Fe	Mo
12	0.01	0.02	18.45	53.43	0.01	18.83	2.91
29	0.07	0.08	17.97	53.92	0.71	17.61	2.96
60	<0.01	<0.01	17.85	53.50	0.01	18.46	2.88
100	<0.01	<0.01	17.87	53.55	0.01	18.46	2.88

Alloy	P	W	V	Nb	Ti	Al	B, ppm	C, ppm
12	0.002	0.001	0.03	4.86	0.97	0.46	12	120
29	0.007	0.07	0.02	5.12	0.94	0.47	29	225
60	<0.003	<0.01	0.02	5.33	0.99	0.54	60	40
100	<0.003	0.01	0.02	5.33	0.99	0.54	100	40

Alloy	Cu	Ta	Hf	Ag, ppm	Pb, ppm	Bi, ppm	Ca, ppm	Mg, ppm
12	0.001	0.004	0.004	<5	<3	<0.3	<50	36
29	0.02	0.005	0.004	<5	<3	<0.3	<50	10
60	0.02	<0.01		2	<1	<0.1		100
100	0.02	<0.01		1	<1	0.1		57

Alloy	S, ppm	Sn, ppm	Cd, ppm	Sb, ppm	O, ppm	N, ppm	Zr
12	10	<20	<50	<20	3	2	0.001
29	3	<20	<50	<20	1	65	0.001
60	4	<5	…	…	<5	22	<0.01
100	<3	<5	…	…	8	22	<0.01

at 718 °C for 8 h, cooled to 621 °C at a rate of 50 °C/h, and held at 621 °C for 8 h before air cooling to RT.

2.2 Fracture Toughness Test and Fractographic Analysis

The plane-strain fracture toughness values (K_{IC}) were determined by tests done in accordance with ASTM Standard E399-90 using three samples for each condition. The samples tested did not satisfy the requirement of thickness specified in ASTM E399-90 due to the relatively good ductility of the material, and hence, the fracture toughness values were designated K_Q. The elastic-plastic J integral tests were, therefore, performed to obtain valid fracture toughness data in accordance with ASTM E1820-99a, using the recommended procedure for establishing J_{1C} outlined by Landes and Begley (Ref 21). The single-specimen J-R curve technique was used to characterize the ductile fracture toughness behavior and establish J_{1C} values of alloys as a function of B and C concentrations using three samples per condition. J_{IC} values were measured using deeply cracked specimens, which were fatigue precracked to $a/W = 0.65$ (a is the crack length) at a maximum stress intensity factor of 30 MPa$\sqrt{m}$. In contrast, K_Q specimens were fatigue precracked to $a/W = 0.5$.

Fracture toughness (K_Q and J_{1C}) tests were conducted at RT and 650 °C in air with an INSTRON 8502 servo-hydraulic testing system (Instron, Canton, MA) fitted with a radiation furnace. K_Q tests were performed under load control criterion at a loading rate of 0.2 kN/s, and J_{IC} tests were performed under stroke control criterion at a crosshead rate of 2.0×10^{-4} mm/s. Displacements were measured on the load-line by an INSTRON high temperature extensometer, which consisted of two arms, mounted one above the other and pivoted about their centers. The forward end of each arm was placed in contact with the specimen, and the rearward end of each arm was connected to an encapsulated resistive strain gauge sensor. Strain or displacement experienced by the specimen caused the extensometer arms to move. This movement was transmitted to the sensor and converted to an electrical signal, proportional to the specimen strain, which was used for the measurement and control purposes. During each test, the load-line displacement was recorded continuously using an X-Y recorder as a function of load. During J_{IC} testing, the specimens were repeatedly unloaded to an amount less than 20% of the current load at intervals of approximately 0.04-0.06 mm crack opening displacement on the load line. Tests were stopped after approximately 1.5 mm of stable crack growth, during which 12-16 unloading-reloading cycles were accomplished.

A JEOL JSM-5200LV (Japan Electron Optics, Ltd., Tokyo, Japan) scanning electron microscope (SEM) (Japan Electron Optics, Ltd., Tokyo, Japan) equipped with an ultrathin window energy dispersive spectrometer (EDS) was used for microstructural analysis and fractography to identify the cracking mechanism after fracture toughness tests at RT and 650 °C. Microstructures were also examined using a JEOL JEM-2000FX transmission electron microscope (TEM) equipped with an EDS microanalytical system.

3. Results

3.1 Microstructures and Tensile Properties of the Heat-Treated IN 718

The microstructures of the heat-treated IN 718 consisted of equiaxed grains with a significant volume fraction of δ-phase, some intragranular carbides and small grain boundary carbides, as shown in Fig. 1. Typical SEM backscatter electron images of the microstructure and EDS spectra of heat-treated alloys, with 29 ppm B and 225 ppm C, prior to deformation is shown in Fig. 1(a)-(e). Grain boundaries are seen to be extensively decorated with particles of various morphologies, ranging from globular to needlelike. Carbides on grain boundaries were observed to have a globular morphology, as indicated by an arrow in Fig. 1(a), and they were enriched in Nb, Cr, Ti and Fe (Fig. 1b), whereas the carbide inside the grain (Fig. 1c) were mainly enriched in Nb and Ti elements, as shown in Fig. 1(d). Carbides were observed in all four alloys, and, as expected, their volume fraction increased with increasing C level. Some borides were observed at the grain boundaries, as indicated by an arrow in Fig. 1(e). The borides were also enriched in Nb and Ti (Fig. 1f). TEM examination showed that, as a precipitation hardened superalloy, the CHT heat treated specimens were primarily strengthened by γ″ precipitates of about 30 nm in diameter and 5 nm in thickness, as shown in the bright-field TEM image in Fig. 2(a) and in the dark-field TEM image (Fig. 2b) obtained with (010) superlattice reflection (Fig. 2c and d). The γ″ phase has a DO_{22} ordered body-centered tetragonal structure. It is based on Ni_3Nb phase and possesses a disklike morphology having a cube-cube relationship with the parent face-centered-cubic (fcc) γ matrix: $[001]_{\gamma''} \| \langle 001 \rangle_{\gamma}$ and $\{100\}_{\gamma''} \| \{100\}_{\gamma}$. The alloy also contains a smaller amount of spherical γ′ precipitate particles, identified by an arrow in Fig. 2(b), which is an ordered fcc $L1_2$ type $Ni_3(Ti,Al)$ phase.

The tensile properties of IN 718, with different concentrations of B and C at RT and 650 °C are given in Table 2, and Fig. 3(a) and (b) show the effect of B on the yield strength ($\sigma_{0.2}$), the ultimate tensile strength (σ_{UTS}), and elongation (δ) at

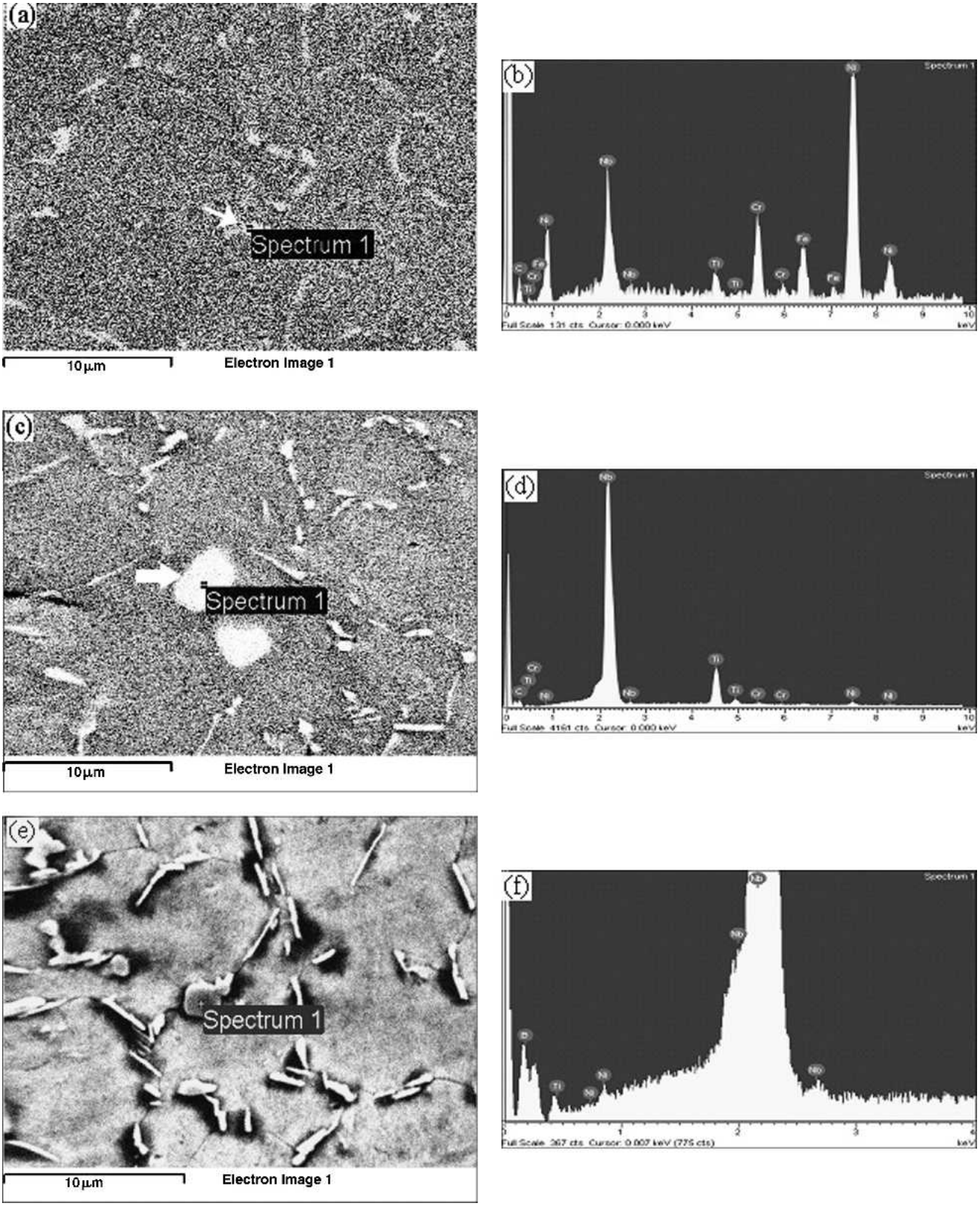

Fig. 1 SEM-EDS analysis of the undeformed specimens for the heat-treated IN 718 with 29 ppm B and 225 ppm C: (a) SEM backscatter electron image containing carbides at grain boundaries, (b) EDS showing the grain boundary carbide, (c) SEM backscatter electron image containing intragrain carbides, (d) EDS showing the intragrain carbide, (e) Secondary electron image showing the structure consisting of equiaxed grains with a significant number of δ phase and boride at grain boundaries, and (f) EDS showing the grain boundary boride

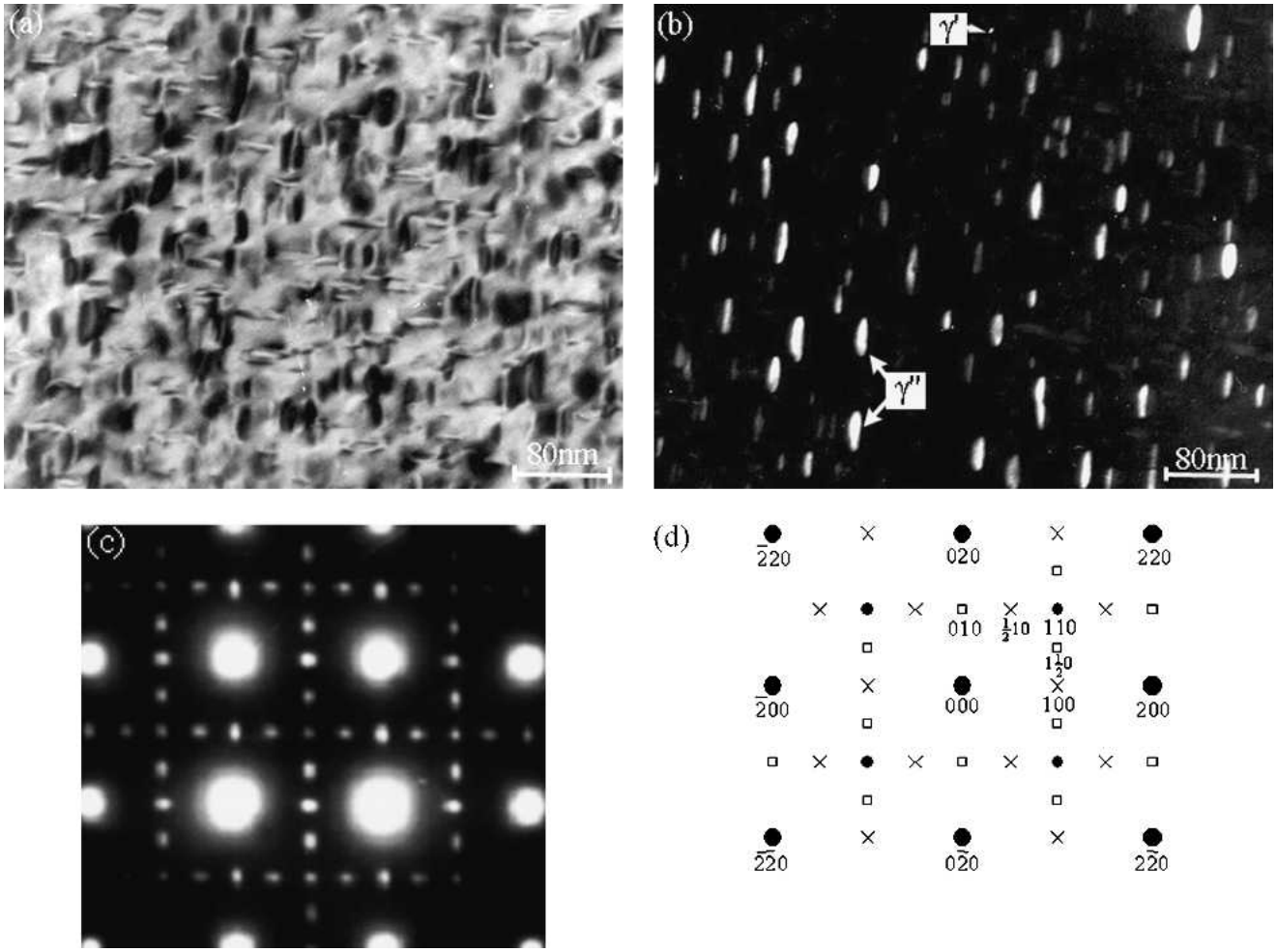

Fig. 2 TEM micrographs of the heat-treated IN 718 showing the presence of γ″ and γ′ precipitates: (a) bright-field image with [001] orientation, (b) dark field image with [001] orientation with 010 reflection showing γ″ and γ′ precipitates, (c) SAD pattern with [001] zone axis, and (d) key corresponding to the SAD pattern in (c)

Table 2 Tensile properties of heat-treated IN 718 with different concentrations of B and C at RT and 650 °C

Test temperature, °C	B, ppm	C, ppm	$\sigma_{0.2}$, MPa	σ_{UTS}, MPa	δ, %
25	12	120	1190	1486	26
	29	225	1244	1493	23
	60	40	1018	1610	30
	100	40	1005	1529	27
650	12	120	999	1122	28
	29	225	1059	1200	20
	60	40	1054	1276	31
	100	40	1028	1203	29

RT and 650 °C, respectively. It is seen that an increase in B increased the value of yield strength at RT, but the ductility was somewhat reduced. By comparing the yield strength of the 60 and 100 ppm B alloys that contained the same amount of C, 40 ppm, it is seen that B does not influence the values significantly. At 650 °C, the yield strength and ductility were not significantly affected by a change in concentration of B and C. In summary, at RT, the yield strength of the 29 ppm B and 225 ppm C was highest, and the ductility was lowest; at 650 °C, however, the yield strengths of all the four alloys were comparable, but the ductility of the 29 ppm B and 225 C alloy was significantly smaller.

3.2 Effects of Boron and Carbon Concentrations on the Fracture Toughness of IN 718

3.2.1 K_Q Values. Fracture toughness was initially measured for IN 718 with different concentrations of B and C at RT and 650 °C; however, as stated earlier, the 12.7 mm thick samples used in this study did not meet the thickness requirement of ASTM specification, E399-90. Therefore, the fracture toughness values reported are designated as K_Q values, which may be somewhat higher than the true plane-strain fracture toughness (K_{IC}) values due to thickness effects (Ref 22, 23). The K_Q values obtained are illustrated in Fig. 4 and tabulated in Table 3. It is seen that at RT the value of K_Q increased from 130.8 to 137.4 MPa$\sqrt{m}$ as B increased from 12 to 29 ppm and C increased from 120 ppm to 225 ppm. However, the fracture toughness dropped down to 109.2 MPa$\sqrt{m}$ as the B concentration increased from 29 to 60 ppm and C concentration decreased from 225 to 40 ppm. In contrast, the value of K_Q increased continuously at 650 °C in these alloys. Among the four alloys, the alloy with 60 ppm B and 40 ppm C exhibited the highest K_Q value of 117.3 MPa$\sqrt{m}$ at 650 °C. As the B

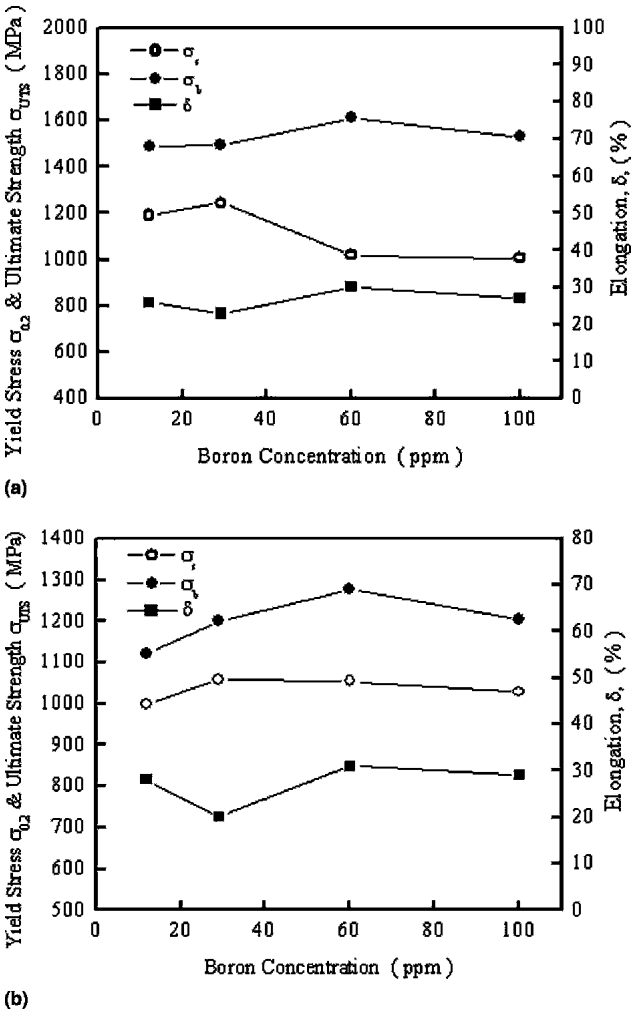

Fig. 3 Effect of B concentrations on the tensile properties of IN 718 at (a) RT and (b) 650 °C

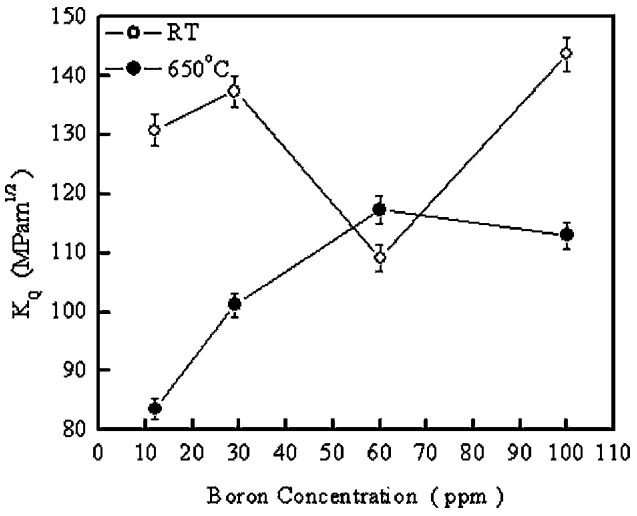

Fig. 4 Effect of B concentrations on the fracture toughness K_Q.

concentration further increased to 100 ppm, the value of K_Q increased to 143.7 MPa√m at RT, which is even higher than that observed in the alloy with 29 ppm B and 225 ppm C; K_Q decreased slightly to 113.0 MPa√m at 650 °C.

Table 3 Fracture toughness (K_Q) of IN 718 with different concentrations of B and C at RT and 650 °C

Test temperature, °C	B, ppm	C, ppm	K_Q, MPa√m
25	12	120	130.8
	29	225	137.4
	60	40	109.2
	100	40	143.7
650	12	120	83.6
	29	225	101.2
	60	40	117.3
	100	40	113.0

Further analysis showed that the improvement in the fracture toughness of these alloys due to the B addition was greater at 650 °C than at RT. The greatest effect of the B addition on the fracture toughness at 650 °C occurred with an initial increase in the concentration of B from 12 to 29 ppm, which increased the fracture toughness from 83.6 to 101.2 MPa√m, an increase of 21%. The fracture toughness further increased to 117.3 MPa√m, an increase of 16%, by an increase in B concentration to 60 ppm B, whereas the C concentration reduced from 225 to 40 ppm. This means that improvement in the K_Q values at 650 °C due to the B addition is significant in this range of B concentration. However, at RT, the alloy with 60 ppm B exhibited a distinct reduction in the K_Q values, which is in agreement with a decrease in $\sigma_{0.2}$ value, as shown in Fig. 3(a). Further analysis suggests that the reduction in K_Q value is consistent with the dramatic decrease in C concentration in this alloy. This implies that the C concentration affected significantly the $\sigma_{0.2}$ and K_Q values of IN 718 at RT. The K_Q value at RT was observed to be even lower than that observed at 650 °C in the alloy with 60 ppm B and 40 ppm C.

3.2.2 J_{IC} Values. The *J-R* curves were constructed by plotting *J*-integral values against the corresponding crack-extension (Δa) values and fitting the J-Δa data with a power-law regression line. The J_{IC} toughness was the value of *J* at the intersection of the power-law curves with the 0.2 mm offset blunting line:

$$\Delta a = \frac{J}{4\sigma_f} + 0.2 \qquad \text{(Eq 1)}$$

where σ_f is the flow strength defined as the average of the $\sigma_{0.2}$ and σ_{UTS}.

The J_{1C} values obtained at RT and 650 °C, as a function of B and C concentrations, are illustrated in Fig. 5(a) and (b), respectively, and tabulated in Table 4. The equivalent critical stress-intensity factors (K_{IC}) were computed from the experimental J_{1C} values using the equation:

$$K_{IC} = \sqrt{\frac{EJ_{IC}}{1-\nu^2}} \qquad \text{(Eq 2)}$$

where E is the Young′s modulus and ν is the Poisson's ratio of the material. The K_{IC} values obtained using Eq 2 are also included in Table 4 and plotted in Fig. 6.

Tests at RT revealed that the alloy with 12 ppm B and 120 ppm C had a J_{IC} value of 64.5 kJ/m^2. It increased from 64.5 kJ/m^2 to 72.9 kJ/m^2, an increase of 13%, as the B concentration

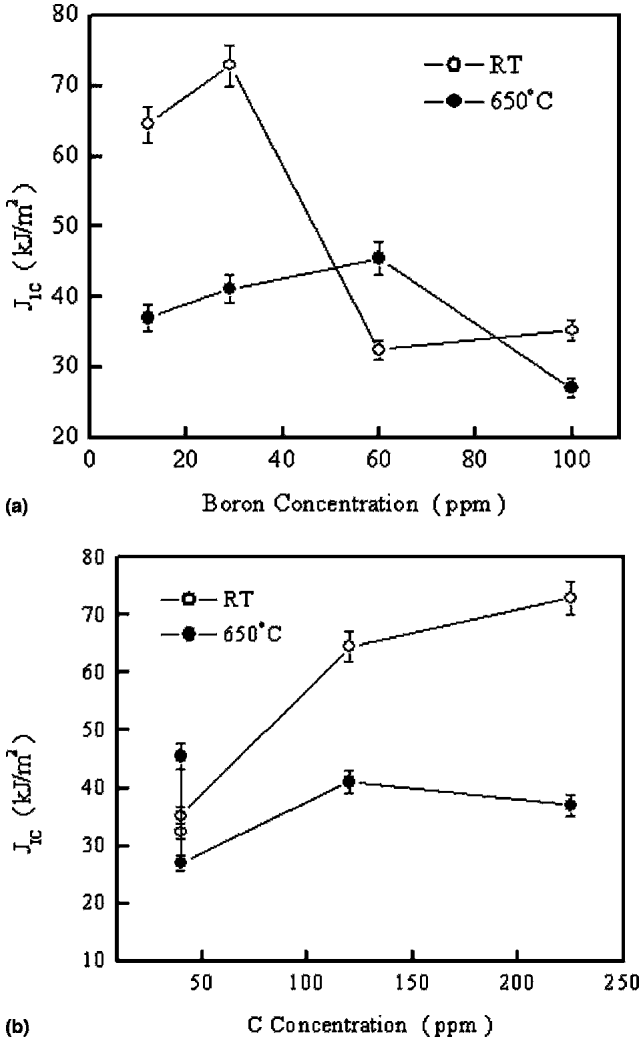

Fig. 5 Effect of B and C concentrations on the fracture toughness J_{1C} in IN 718 at RT and 650 °C: (a) J_{IC} versus B concentration and (b) J_{IC} versus C concentration

Table 4 Fracture toughness (J_{1C}) of IN 718 with different concentrations of B and C at RT and 650 °C

Test temperature, °C	B, ppm	C, ppm	J_{1C}, kJ/m^2	K_{1C}, MPa√m
25	12	120	64.5	118.8
	29	225	72.9	126.3
	60	40	32.4	84.2
	100	40	35.2	87.8
650	12	120	37.0	81.0
	29	225	41.1	85.3
	60	40	45.5	89.8
	100	40	27.0	69.2

increased from 12 to 29 ppm and C increased from 120 to 225 ppm. However, there was a considerable reduction in the fracture toughness, J_{IC} value, (to 32.4 kJ/m^2) as the B concentration increased to 60 ppm and the C concentration decreased to 40 ppm, which is in agreement with the observed reduction in the value of K_Q (Fig. 4). When the B concentration increased to 100 ppm and the C concentration remained at 40 ppm, a slight increase in J_{IC} values was observed, compared with the alloy

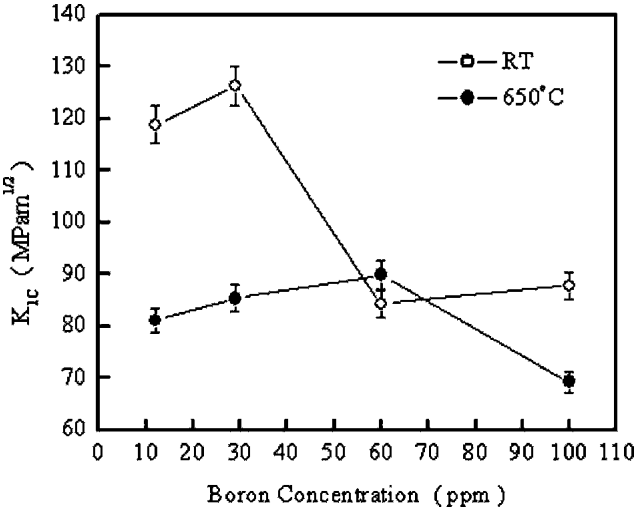

Fig. 6 Effect of B concentrations on the fracture toughness K_{IC}

with 60 ppm B (Fig. 5a). Therefore, of all the four alloys the one with 29 ppm B and 225 ppm C had the highest J_{IC} value, whereas the alloy with 60 ppm B and 40 ppm C had the lowest J_{IC} value among the four alloys tested at RT (Fig. 5a). At 650 °C, the J_{IC} values increased continuously as the B concentration increased from 12 to 60 ppm. However, a further increase in B concentration from 60 to 100 ppm led to a decrease in J_{IC} values. Therefore, the alloy with 60 ppm B and 40 ppm C displayed the highest J_{IC} value at 650 °C. The effect of C concentration on the fracture toughness of IN 718 is shown in Fig. 5(b). It is seen that the J_{IC} values increased monotonically with increasing C concentration at RT, whereas the C concentration had a relatively weak effect on J_{IC} at 650 °C.

The same trend in the variation of J_{IC} and K_{IC} values was observed (Fig. 5a and Fig. 6), similar to the trend in the variation of the measured K_Q values (Fig. 4).

3.3 Fractography

To gain insight into the effect of B and C on the fracture mechanism, the fracture surfaces of K_Q and J_{IC} tested specimens were examined by SEM. Typical fractographs of K_Q and J_{IC} specimens tested at RT are shown in Fig. 7(a)-(d) and 8(a)-(d), respectively. The fracture surface topography consisted of dimples and shear-stretch markings. The large dimples were observed to be associated with fractured carbide particles, as indicated by arrows in Fig. 7(b) and (d). Their growth seems to have involved a considerable amount of plastic deformation, as evidenced by extensive plastic deformation traces on the surfaces of the very deep dimples, indicated by arrows in Fig. 8(a)-(d). The only discernible difference in the fracture surface micromorphologies in these alloys was the size and distribution of dimples. As the B and C concentration increased, the dimple size seemed to decrease slightly (Fig. 7a and b). This indicates that the amount of void growth decreased with increasing B and C concentration. Extensive plastic deformation traces in the shear-stretch regions on the fracture surface in the alloy with 100 ppm B (Fig. 7d) indicates that a large amount of plastic deformation is required to propagate a crack in the alloy with a higher concentration of B. A comparison of the fracture surfaces of the K_Q samples and J_{IC} samples with similar B concentrations showed that more local-

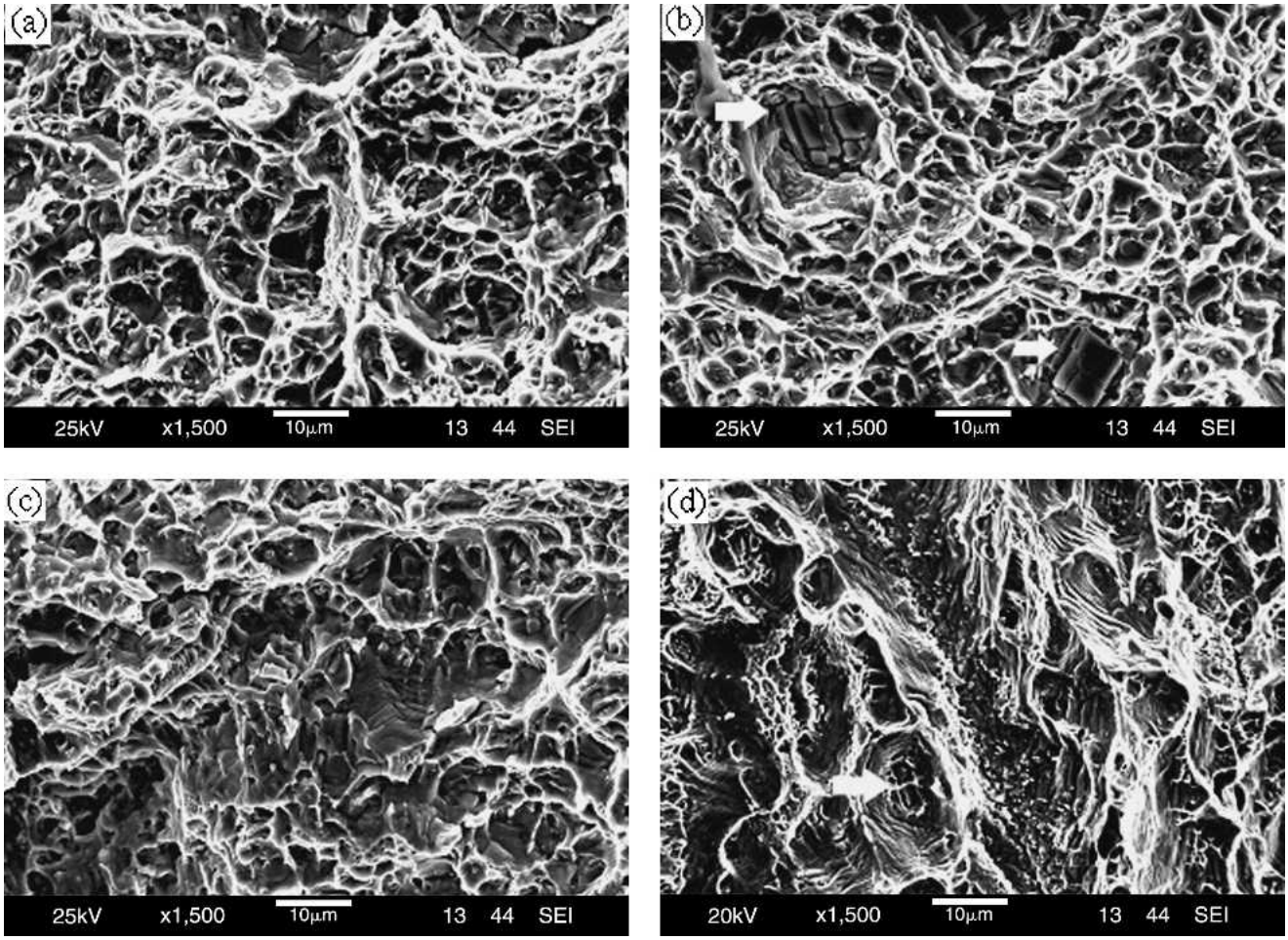

Fig. 7 Typical fracture surfaces of IN 718 with different concentrations of B and C after K_Q tests at RT: (a) 12 ppm B and 120 ppm C, (b) 29 ppm B and 225 ppm C, (c) 60 ppm B and 40 ppm C, and (d) 100 ppm B and 40 ppm C

ized plasticity occurred in the J_{IC} fracture toughness tested samples than in the K_Q samples, specifically in the alloy with 100 ppm B, as shown in Fig. 7(d) and 8(d). In summary, at RT, the fracture process seems to have consisted of the formation and growth of dimples around second phase particles and final coalescence or linkage of these dimples.

At 650 °C, the representative fracture surface morphologies observed in the K_Q and J_{IC} tested specimens are shown in Fig. 9(a)-(d) and 10(a)-(d), respectively. Intergranular fracture coupled with the secondary cracks was the predominant character in the alloys with 12 and 29 ppm B (Fig. 9a, 9b, 10a, and 10b). As the B concentration increased, the intergranular fracture was still the primary character in the alloy with 60 ppm B in the K_Q tested specimen, but some plastic deformation traces were also observed (Fig. 9c). However, the fraction of the plastic shear traces was observed to increase, and secondary cracks were seldom observed on the fracture surface in the J_{IC} tested specimen (Fig. 10c). This indicates that a significant amount of localized plastic deformation occurred, characterized by tear ridges, dimples, and microvoids that formed at slip band facet steps (Fig. 10c). Furthermore, a transition in the nature of fracture from intergranular cracking to ductile tearing occurred as the B concentration increased from 60 to 100 ppm. At 650 °C, the fracture surface of the specimens with 100 ppm B was mainly characterized by a combined mode of transgranular fracture with tearing ridges (Fig. 9d and 10d). On closer examination, the fracture surfaces of J_{IC} samples showed a more localized plasticity than that observed in the K_Q samples of similar B concentrations at 650 °C as well.

4. Discussion

4.1 Influence of Boron Addition

Boron is an essential ingredient in IN 718 superalloy, and the addition of B even at parts-per-million levels remarkably enhances its fracture toughness at RT and 650 °C. The improvement in the fracture toughness of IN 718 by B addition is related to the increased grain boundary cohesion caused by B segregation, specifically at 650 °C (Ref 7, 15). Stress and strain concentrations in the grain boundary region, induced by the lack of a sufficient number of slip systems or induced by the misorientation between the grains, can be accommodated by either intergranular cracking or transgranular cracking, depending on the cohesive strength of the grain boundaries relative to that of the bulk material. Boron containing precipitate particles were observed at grain boundaries (Fig. 1e), and segregation of B at grain boundaries was observed by secondary ion mass spectroscopy (SIMS) analysis in earlier studies on the weldability of IN 718 (Ref 9-12). This observation supports the views that B segregation has a beneficial effect on the cracking resistance of IN 718 via the increased grain cohesion at 650 °C

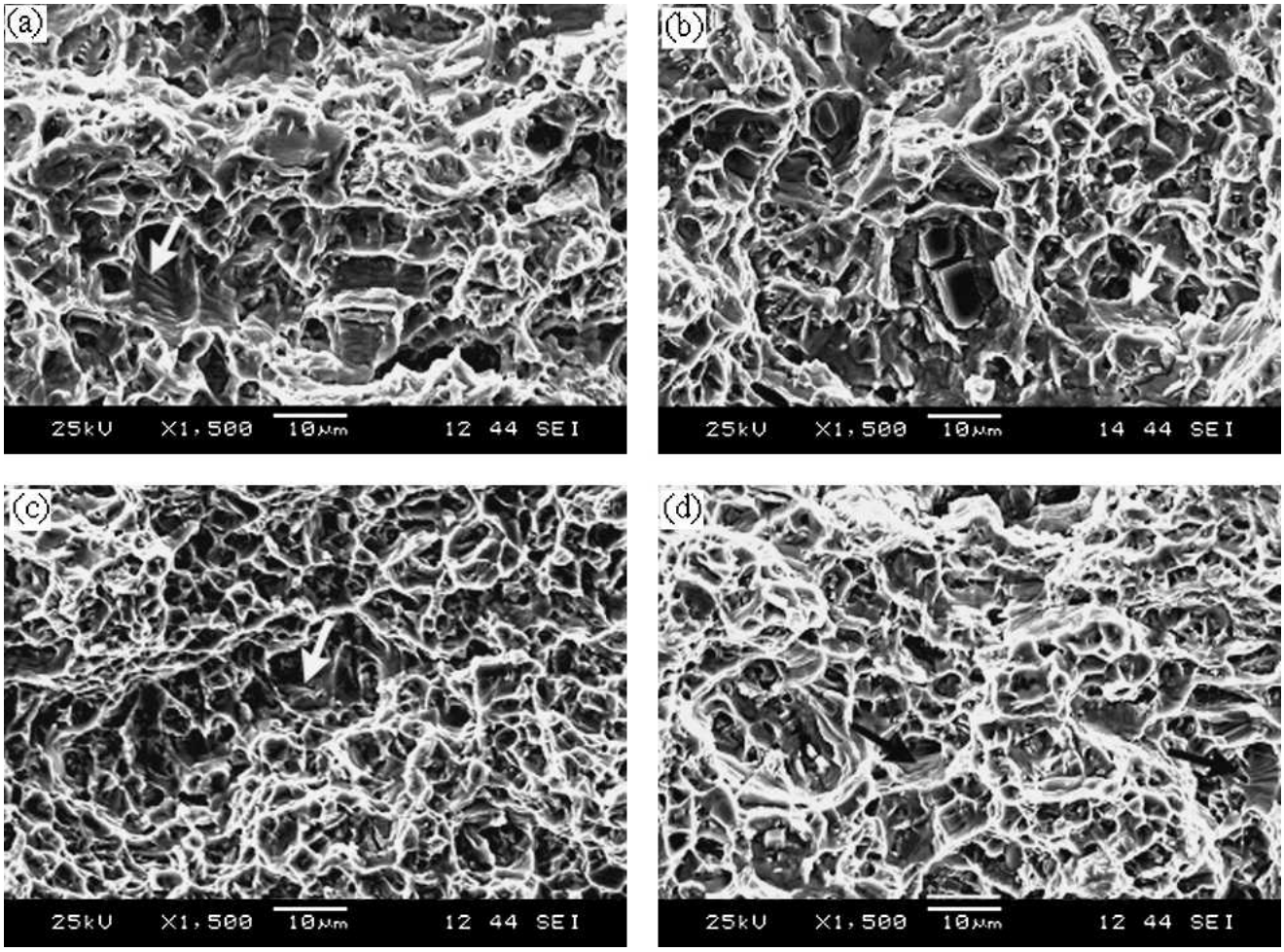

Fig. 8 Typical fracture surfaces of IN 718 with different concentrations of B and C after J_{1C} tests at RT: (a) 12 ppm B and 120 ppm C, (b) 29 ppm B and 225 ppm C, (c) 60 ppm B and 40 ppm C, and (d) 100 ppm B and 40 ppm C

(Ref 7, 17). The relatively weaker grain boundaries in IN 718 with lower B concentration result in intergranular fracture, as observed in the alloy with 12 and 29 ppm B at 650 °C (Fig. 9a, 9b, 10a, and 10b). Fractographic observations suggest that the grain boundary strength was enhanced with an increase in B concentration of up to 60 ppm, as evidenced by the decreasing component of intergranular cracking on the fracture surface at 650 °C (Fig. 9c and 10c). Entirely transgranular fracture was observed in the alloy with the highest B concentration of 100 ppm (Fig. 9d and 10d). This signifies that, when the B concentration increased to 100 ppm, grain boundaries were not the preferential path for microcrack propagation due to their strengthening by B, even at the test temperature of 650 °C.

The improved fracture toughness by the B addition is also associated with the stabilization of grain-boundary constituents (Ref 1, 24, 25). IN 718 superalloy with a lower B level was likely to be subjected to a rapid agglomeration of $M_{23}C_6$ and γ' precipitates and intergranular microcracking at grain boundaries (Ref 24, 25). Brittle fracture would then occur by the coalescence of microcracks. However, the addition of B may lower the tendency of rapid agglomeration of $M_{23}C_6$ and γ' particles, thereby reducing the possibility of intergranular cracking, and improve the fracture resistance. It has been proposed that intergranular microcracking at the grain boundaries transverse to applied stress is inhibited in B containing alloys because B stabilizes the fine γ' precipitates and prevents the formation of precipitate-denuded zones (Ref 24, 25). As the B concentration increases further, excess B would be tied up by molybdenum, titanium, chromium, niobium, and nickel to form a complex boride (Ref 9), which could act as a potential microcrack initiation site. As a result, the fracture toughness of IN 718 with very high B levels decreased by the early initiation of cracks along the interfaces between the borides and matrix.

4.2 Influence of Carbon Addition

It was observed that the RT J_{IC} values increased monotonically with increasing C concentration. However, the C addition did not appear to result in an improvement in the J_{IC} values at 650 °C, as seen in Fig. 5(b). In nickel-base superalloys, the C addition generally results in the formation of precipitates such as the MC, M_7C_3, and $M_{23}C_6$ carbides (Ref 2, 4, 6). Although the solubility of C in nickel is appreciable, the presence of stable carbide-forming elements, such as niobium, titanium and chromium, results in a very small amount of C in solution in the matrix. Therefore, an increase in the concentration of C results in the formation of intergranular and intragranular carbide precipitates. The former pin the grain boundaries and thus inhibit grain boundary sliding (Ref 2, 4, 24). This grain boundary strengthening mechanism is expected to be more apparent

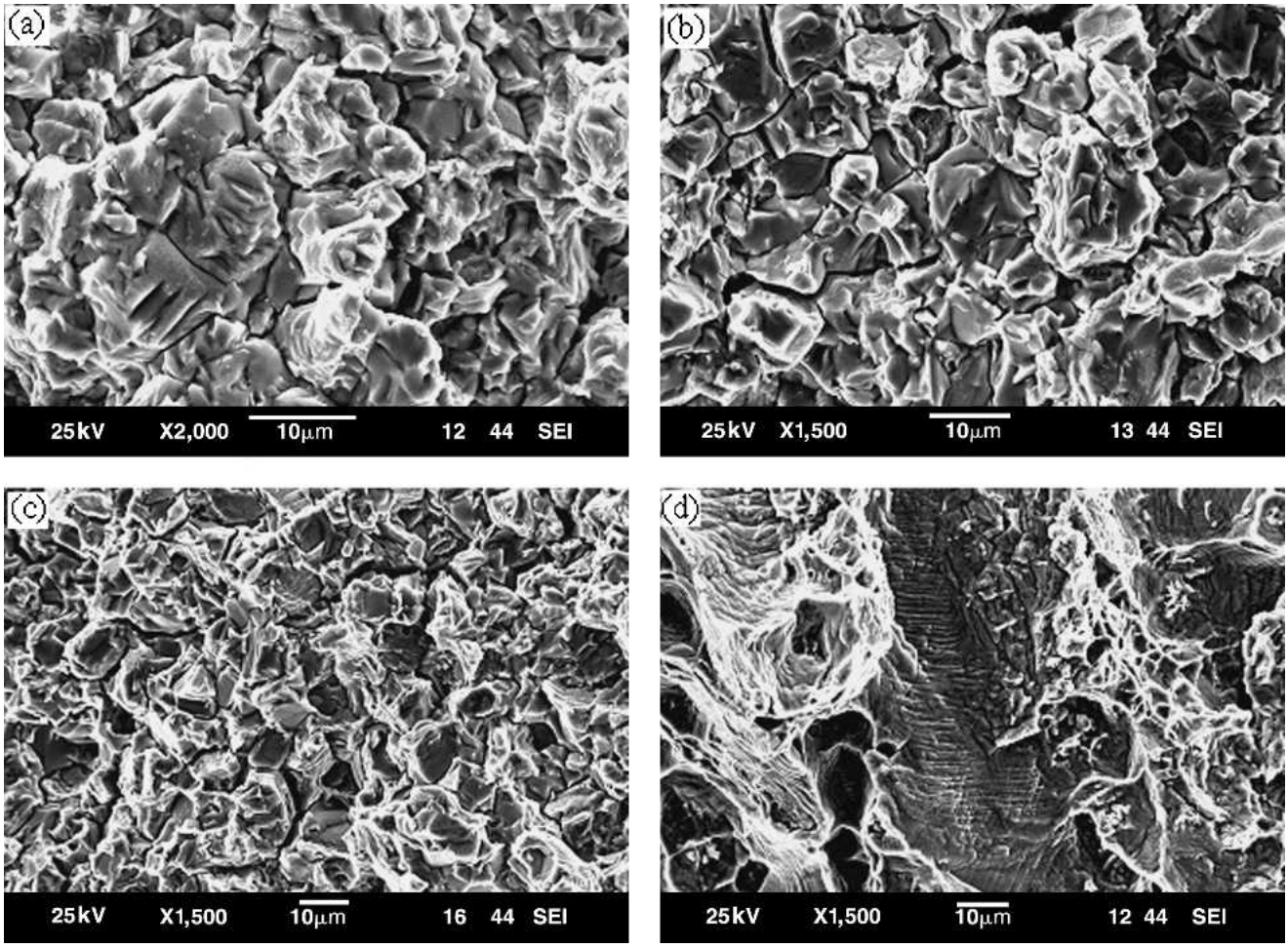

Fig. 9 Typical fracture surfaces of IN 718 with different concentrations of B and C after K_Q tests at 650 °C: (a) 12 ppm B and 120 ppm C, (b) 29 ppm B and 225 ppm C, (c) 60 ppm B and 40 ppm C, and (d) 100 ppm B and 40 ppm C

at elevated temperatures, where grain boundary sliding becomes significant. The latter is beneficial for fracture properties through blocking of the plastic deformation, as evidenced by a decrease in the values of $\sigma_{0.2}$ with decreasing concentration of C (Table 2). EDS analysis revealed the presence of carbide precipitates along grain boundaries and within the grains (Fig. 1a and c). B, however, was present in the form of both particles and as segregation at grain boundaries. In other words, a significant amount of B is believed to be present at the grain boundaries and significantly increased their strength, whereas C did not. Therefore, C has little effect on the grain boundary strength at 650 °C. The beneficial effect of C is derived primarily from the intergranular and intragranular carbides, which formed during the heat treatment and improved the alloy strength via blocking the plastic deformation. However, the effect of C is limited when the intergranular cracking becomes the primary fracture model and the grain boundary sliding does not play a significant role during fatigue deformation of IN 718 at 650 °C.

4.3 Influence of Interaction between Boron and Carbon

Fracture surfaces exhibited microvoid coalescence in the alloys tested at RT. Carbides were always observed to be present on the fracture surfaces with void growth around them. The reason for the RT fracture resistance of the alloy with 60 ppm B is lower than that of the other alloys may be caused by a deficiency in primary carbides due to the lower C concentration. The lower volume fraction of carbides would also result in a reduction in yield stress ($\sigma_{0.2}$) in this alloy, as seen in Table 2. With a further increase in B concentration from 60 to 100 ppm, the excess B would compensate the loss of fracture toughness caused by the lower C concentration (40 ppm C) in the alloy.

B has a stronger influence on improving the fracture toughness J_{IC} and K_{IC} of the alloy tested at 650 °C in comparison with that observed at RT. This indicates that the role of B is exerted through its effect on the grain boundary behavior. Because B segregated on grain boundaries, the grain boundary strength or cohesion improved appreciably at 650 °C, as evidenced by the change in the appearances of fracture surface, shown in Fig. 9 and 10, where the relative amount of transgranular fracture increased with increasing B concentration. The effect of B on grain boundary cohesion is stronger than the effect of carbide pinning, thus giving rise to an effect on the J_{IC} and K_{IC} values stronger than the effect of C at 650 °C. The fractographic studies also showed that the lower fracture toughness in IN 718 with lower B concentration is associated with the transition of fracture surface morphologies from ductile tearing to intergranular cracking at 650 °C.

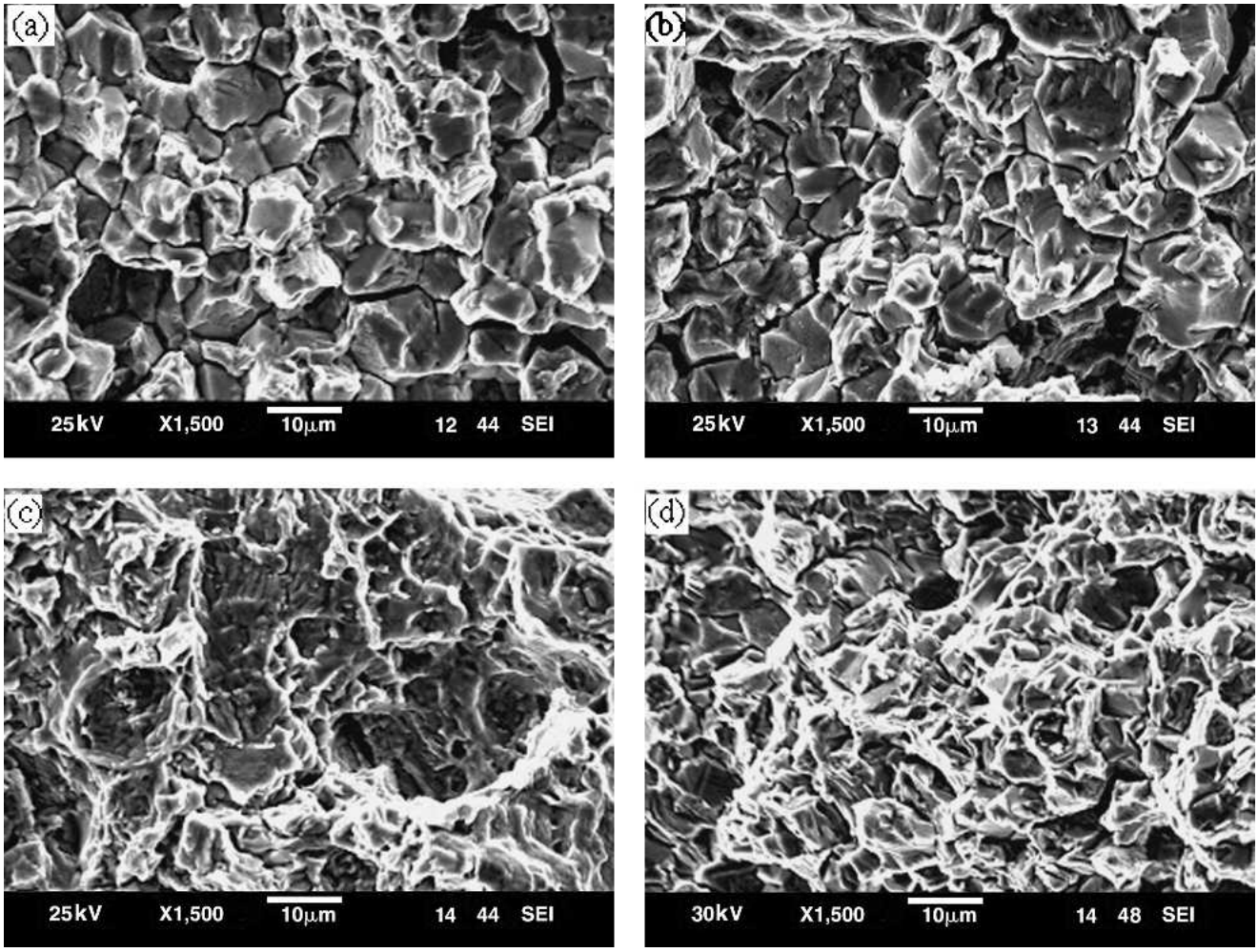

Fig. 10 Typical fracture surfaces of IN 718 with different concentrations of B and C after J_{1C} tests at 650 °C: (a) 12 ppm B and 120 ppm C, (b) 29 ppm B and 225 ppm C, (c) 60 ppm B and 40 ppm C, and (d) 100 ppm B and 40 ppm C

5. Conclusions

The fracture toughness of IN 718 at room temperature as well as at 650 °C increased as the B concentration increased from 12 to 29 ppm, and the C concentration increased from 120 to 225 ppm. When the B concentration increased to 60 ppm and the C concentration decreased to 40 ppm, the fracture toughness value at RT was reduced, and the alloy had the highest fracture toughness value among the four alloys with different concentrations of B and C at 650 °C. A further increase in the B concentration to 100 ppm while C concentration was maintained at 40 ppm gave rise to an increase in the fracture toughness at RT, but a decrease at 650 °C.

At RT, the formation and coalescence of microvoids were observed to be the predominant fracture mechanism of IN 718 superalloy with different concentrations of B and C. At 650 °C the fracture mode changed from intergranular fracture in the alloy with the low B concentration to transgranular fracture coupled with the formation of some fine dimples in the alloy with the high B concentration.

The addition of B caused segregation of B to the grain boundaries and precipitation of boride particles. As a result, the role of B was to hamper intergranular cracking by improving the grain boundary cohesion and stabilizing grain boundaries. In contrast, the addition of C generally resulted in the formation of sparsely distributed carbide precipitates at grain boundaries and within the grains, which led to an increase in the fracture toughness by increasing the resistance to the plastic deformation at RT.

Acknowledgment

The authors would like to thank the Natural Sciences and Engineering Research Council of Canada for the financial support.

References

1. R.T. Holt and W. Wallace, Impurities and Trace Elements in Nickel-base Superalloys, *Int. Metals Rev.,* Vol 21, 1976, p 1-24
2. T.J. Garosshen, T.D. Tillman, and G.P. McCarthy, Effects of B, C, and Zr on the Structure and Properties of a P/M Nickel Base Superalloy, *Metall. Trans. A,* Vol 18, 1987, p 69-77
3. F.T. Furillo, J.M. Davidson, J.K. Tien, and L.A. Jackman, The Effects of Grain Boundary Carbides on the Creep and Back Stress of a Nickel-base Superalloy, *Mater. Sci. Eng.,* Vol 39, 1979, p 267-273
4. T.J. Garosshen and G.P. McCarthy, Low Temperature Carbide Precipitation in a Nickel Base Superalloy, *Metall. Trans. A,* Vol 16A, 1985, p 1213-1223
5. C.C. Law and M.J. Blackburn, Creep-Rupture in Powder Metallurgi-

cal Nickel-Base Superalloys at Intermediate Temperatures, *Metall. Trans. A,* Vol 11, 1980, p 495-507
6. M.A. Burke, J. Greggi, Jr., and G.A. Whitlow, The Effect of Boron and Carbon on the Microstructural Chemistries of Two Wrought Nickel Base Superalloys, *Scripta Metall.,* Vol 18, 1984, p 91-94
7. W.D. Cao and R.L. Kennedy, Effect and Mechanism of Phosphorus and Boron on Creep Deformation of Alloy 718, *Proceedings of the Coference on Superalloys 718, 625, 706 and Various Derivatives*, E.A. Loria, Ed., TMS, Warrendale, PA, 1997, p 511-520
8. S. Floreen and J.M. Davidson, The Effects of B and Zr on the Creep and Fatigue Crack Growth Behavior of a Ni-Base Superalloy, *Metall. Trans. A,* Vol 14, 1983, p 895-901
9. X. Huang, M.C. Chaturvedi, N.L. Richards, and J. Jackman, The Effect of Grain Boundary Segregation of Boron in Cast Alloy 718 on HAZ Microfissuring—a SIMS Analysis, *Acta Mater.,* Vol 45, 1997, p 3095-3107
10. W. Chen, M.C. Chaturvedi, N.L. Richards, and G. McMahom, Grain Boundary Segregation of Boron in Inconel 718, *Metall. Mater. Trans. A,* Vol 29, 1998, p 1947-1954
11. X. Huang, M.C. Chaturvedi, and N.L. Richards, Effect of Homogenization Heat Treatment on the Microstructure and Heat-Affected Zone Microfissuring in Welded Cast Alloy 718, *Metall. Mater. Trans. A,* Vol 27, 1996, p 785-790
12. H. Guo, M.C. Chaturvedi, N.L. Richards, and G.S. McMahom, Interdependence of Character of Grain Boundaries, Intergranular Segregation of Boron and Grain Boundary Liquation in Simulated Weld Heat-Affected Zone in Inconel 718, *Scripta Mater.,* Vol 40, 1999, p 383-388
13. M.G. Stout and W.W. Gerberich, Structure/Property/Continuum Synthesis of Ductile Fracture in Inconel Alloy 718, *Metall. Trans. A,* Vol 9, 1978, p 649-658
14. W.J. Mills, The Effect of Heat Treatment on the Room Temperature and Elevated Temperature Fracture Toughness Response of Alloy 718, A*SEM J. Eng. Mater. Technol.,* Vol 102, 1980, p 118-126
15. M. Clavel and A. Pineau, Fatigue Behaviour of Two Nickel-base Alloys I: Experimental Results on Low Cycle Fatigue, Fatigue Crack Propagation and Substructures, *Mater. Sci. Eng.,* Vol 55, 1982, p 157-171
16. L.A. James, and W.J. Mills, Effect of Heat-Treatment Upon the Fatigue-Crack Growth Behavior of Alloy 718 Weldments—Part I: Macroscopic Behavior, *ASME J. Eng. Mater. Technol.,* Vol 107, 1985, p 34-40
17. T.H. Sanders, Jr.R.E. Frishmuth, and G.T. Embley, Temperature Dependent Deformation Mechanisms of Alloy 718 in Low Cycle Fatigue, *Metall. Trans. A,* Vol 12, 1981, p 1003-1010
18. H.F. Merrick, The Low Cycle Fatigue of Three Wrought Nickel-Base Alloys, *Metall. Trans.,* Vol 5, 1974, p 891-897
19. L. Xiao, D.L. Chen, and M.C. Chaturvedi, Effect of Boron on the Low-Cycle Fatigue Behavior and Deformation Structure of Inconel 718 at 650°C, *Metall. Mater. Trans. A,* Vol 35, 2004, p 3477-3487
20. L. Xiao, D.L. Chen, and M.C. Chaturvedi, Effect of Boron Concentration on Fatigue Crack Propagation Resistance and Low Cycle Fatigue Properties of Inconel 718, *Superalloys 2004,* K.A. Green, H. Harada, T.E. Howson, T.M. Pollock, R.C. Reed, J.J. Schirra, and S. Walston, Ed., TMS, Warrendale, PA, 2004, p 275-281
21. J.D. Landes and J.A. Begley, Test Results from J-Integral Studies: An Attempt to Establish a J_{IC} Testing Procedure, *Fracture Analysis,* ASTM STP 560, 1974, p 170-186
22. J.G. Kaufman, Progress in Fracture Testing of Metallic Materials, *Review of Developments in Plane Strain Fracture Toughness Testing,* W.F. Brown, Jr., Ed., ASTM STP 463, 1970, p 3-21
23. W.S. Walston, N.R.Moody, I.M. Bernstein, and A.W. Thompson, Comparisons of K_{JIC} and K_{IC} Values from Tests on a Single Crystal Nickel-Base Superalloy, *Scr. Metall. Mater.,* Vol 25, 1991, p 1333-1337
24. R.F. Decker and J.W. Freeman, The Mechanism of Beneficial Effects of Boron and Zirconium on Creep Properties of a Complex Heat-Resistant Alloy, *Trans AIME,* Vol 218, 1960, p 277-284
25. K.M. Delargy and G.D.W. Smith, Phase Composition and Phase Stability of a High-Chromium Nickel-Based Superalloy, IN939, *Metall. Mater. Trans. A,* Vol 14, 1983, p 1771-1783